

# CHALMERS



## Finding the Jeffrey Orbits

*Master's Thesis in Complex Adaptive Systems*

Staffan Ankardal

Department of Physics & Engineering Physics  
Non-linear Dynamics & Statistical Physics  
CHALMERS UNIVERSITY OF TECHNOLOGY  
Gothenburg, Sweden 2011  
Master's Thesis 2011:1

---

## Abstract

The Jeffrey orbits define the motion of axissymmetrical particles in shear flow and is thus important in the study of suspensions of particles. In these theses we verify the equations of motion experimentally using glass particles in a reversible flow in a PDMS microchannel and an optical tweezer. We also study the effects of asymmetry on the particles and study the transition from periodic to quasi-periodic orbits for different initial conditions and degrees of asymmetry. A good match with theoretical results are found, but there are some unexplained behaviours when the flow is reversed.

## Acknowledgements

I hereby wish to thank my girlfriend Callie Gibbons for supporting me through the work on this thesis and Alexander Laas for being a tireless and understanding co-worker. I want to thank my supervisors Bernhard Mehlig and Dag Hanstorp for helping with good suggestions. I want to thank all the contributors to the wealth of open source software which I have used to create everything from most of the software to more of the figures and of course this very report.

Staffan Ankardal, Göteborg Sweden INSERT PROPER DATE 3/11/13

# Contents

<b>1</b>	<b>Introduction</b>	<b>1</b>
1.1	Introduction . . . . .	1
1.1.1	Background . . . . .	1
<b>2</b>	<b>Theory</b>	<b>3</b>
2.1	Fluid Dynamics . . . . .	3
2.1.1	Navier Stokes . . . . .	3
2.1.2	Reynold's Number . . . . .	3
2.1.3	Stokes Drag and Stokes's law . . . . .	5
2.2	Euler Angles and our Coordinate System . . . . .	5
2.2.1	Triaxial particles . . . . .	7
2.3	Jeffery Orbits . . . . .	7
2.3.1	Winding Number . . . . .	9
<b>3</b>	<b>Method</b>	<b>12</b>
<b>I</b>	<b>Improvements of Experimental Setup</b>	<b>13</b>
3.1	Improvements . . . . .	14
3.1.1	Particles and Channel . . . . .	14
3.1.2	Automated Tracking . . . . .	17
3.1.3	Aquiring the image . . . . .	17
3.1.4	Removing noise . . . . .	18
3.1.5	Contour detection and selection . . . . .	18
3.1.6	Adjusting the Camera velocity . . . . .	18
3.1.7	Time Considerations . . . . .	19
3.2	Experimental Setup . . . . .	19
3.2.1	List of equipment . . . . .	22
3.2.2	Density matching . . . . .	22

<b>II Measurements and Analysis</b>	<b>23</b>
3.3 Data Analysis . . . . .	24
3.3.1 Particle identification . . . . .	24
3.3.2 Estimation of orientation . . . . .	25
3.3.3 Width compensation . . . . .	26
3.3.4 brushing . . . . .	27
3.3.5 Winding number estimation . . . . .	28
3.3.6 Matching to theoretical orbit . . . . .	28
<b>4 Results</b>	<b>29</b>
4.1 Particle A . . . . .	30
4.2 Particle B . . . . .	34
<b>5 Discussion</b>	<b>36</b>
<b>A Raw data</b>	<b>37</b>

# 1

# Introduction

## 1.1 Introduction

The goal of this thesis is to study and better understand the dynamics of ellipsoidal particles in shear flow, and is a continuation of two previous masters theses [1, 2]. This is done by analysing micrometer length glass particles in a shear flow and comparing this to theoretical models. Before discussing either of these processes more in depth some background and basic theory is needed.

### 1.1.1 Background

The study of particle dynamics in flow began with Einstein's paper from 1905 [3] in which he showed that the viscosity a fluid with suspended spherical particles would increase the viscosity of the fluid and by how much. Jeffrey in his 1922 paper [4] extended these results to ellipsoidal axis-symmetrical ellipsoidal particles as well as derived equations for the orientational dynamics of the particles, in other words how the particles would rotate as a function of time. For systems where inertial effects could be discarded the motion was found to be periodic and depending only on the initial condition of the particle.

Developments on triaxial particles, started with Gierszewski & Chaffey (1978)[5] and was continued by Hinch & Leal (1979)[6] and more recently by Yarin et al in 1993[7]. The dynamics found for axis-symmetric particles by Jeffrey were periodic, but it was shown by Hinch & Leal that some orbits would be doubly periodic, in other words following two separate independent periods. Yarin then was able to use numerical simulations to generate a surface of section [8] for some asymmetric relations between the two minor axes showing that not only was there double periodic or quasi periodic orbits but for sufficiently large asymmetries in axes there would be chaotic orbits. Several other surfaces of were also produced by Johansson (2012)[1] using the same method as Yarin with higher resolution thanks to improvements in computing power. It was there shown that only very small asymmetries on the order of 1% will lead to quasi-periodic motion for some initial conditions.

Experimental studies of these theoretical results were first done by Goldsmith and Mason in 1962[9] who confirmed that the rotation rate matched well with that predicted from Jeffery orbits

### *1.1. INTRODUCTION*

---

but he did not study the actual orbits. Since then most experimental research, such as by Harlen and Koch[10] has been focused on diluted suspensions of particles and the increased viscocity and other properties this causes. Only tangential efforts such as by Tolga[11] were concerned with the Jeffery orbits. A good summary of both theoretical and experimental results was written by Petrie in 1999 [12].

The first dedicated experimental work to try to measure the actual Jeffery orbits and study the orientational dynamics was done by Einarsson et al [13] in 2011. Although there was some promising results, the vast majority of particles were asymmetric to the point of chaotic or highly quasi-periodic. Moreover the width and length of particles both varied great and could not be measured with good accuracy, meaning that the aspect ratio could not accurately be determined. This meant that although the orbits could be qualitatively shown to be similar to some Jeffery orbits no one particle could exhibit both quasi periodic and periodic motion, and there was no particle that could be well matched to a particular orbit.

# 2

## Theory

In order to better understand the results and discussions in this thesis some rather basic results in fluid dynamics, image analysis and other fields need to be understood by the reader.

1) It is however not the focus of this thesis and as such I will try to be as brief as possible, and an experienced reader can safely skip to the next chapter.

OR

2) As the focus of this thesis is experimental I will not go into great detail, but try to briefly motivate and quickly summarize results, and refer the inquisitive reader to more thorough sources. As no recent developments are discussed, readers comfortable in these fields can skip this chapter without any loss in understanding.

### 2.1 Fluid Dynamics

In order to understand the motivations, limitations and behaviour of the experiment we need to know about a few key concepts in fluid dynamics.

#### 2.1.1 Navier Stokes

#### 2.1.2 Reynold's Number

The Reynolds number ( $Re$ ) is a dimensionless number describing the ratio of inertial forces to viscous forces in a flow. For flow in a pipe it is defined as [14]

$$Re = \frac{UL\rho}{\mu} \quad (2.1)$$

where  $U$  is the characteristic velocity of the flow,  $L$  is the characteristic length,  $\rho$  is the density and  $\mu$  is the dynamic viscosity. This is used to estimate the 'regime' of the flow, of which there are two primary types.

1. Laminar flow, where viscous forces dominate over inertial forces

## 2.1. FLUID DYNAMICS

---

2. Turbulent regime where inertial forces dominate.

As the Reynolds number is a ratio between the inertial forces and viscous forces we get more turbulent flow for larger Reynolds numbers, a simple visual characterization of the flow types can be seen in figure 2.1. For  $Re \ll 1$  it is referred to as *Stokes flow* and we can ignore inertial forces completely. This actually means that not only is the flow completely guaranteed to be laminar, but it is time reversible, meaning that reversing the flow any dynamics of the flow and particles in the flow will revert perfectly as well [15].

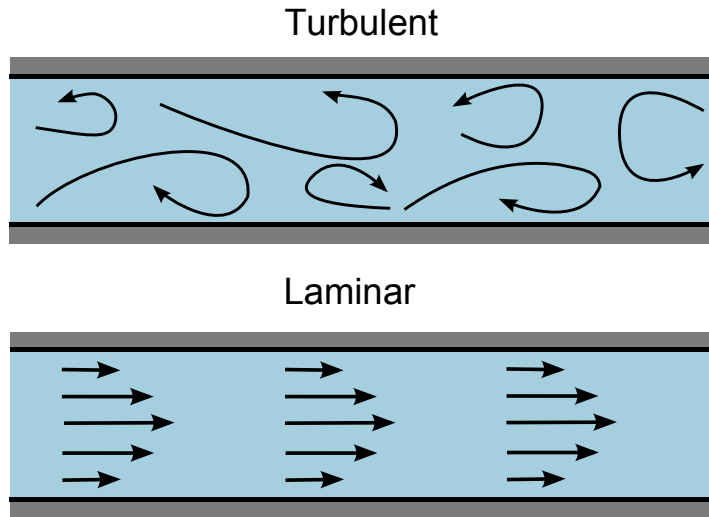


**Figure 2.1:** This shows the principal difference between laminar and turbulent flow

### 2.1.3 Stokes Drag and Stokes's law

The drag force  $F_D$  exerted by a fluid on a spherical particle for  $Re \ll 1$  is found using the so called Stokes's law [16]

$$F_D = 6\pi\mu Rv \quad (2.2)$$

where  $v$  is the velocity of the sphere relative to the fluid,  $\mu$  is the dynamic viscosity and  $R$  is the radius of the sphere. To find the terminal velocity of the sphere we equate this with the gravitational force  $F_G$  acting on the sphere

$$F_G = \Delta\rho g \cdot \frac{4\pi R^3}{3} \quad (2.3)$$

where  $\Delta\rho$  is the difference in density and  $g$  is the specific gravity we find that the terminal velocity of a sinking (or floating) sphere is

$$v_s = \frac{2}{9} \frac{\Delta\rho}{\mu} g R^2 \quad (2.4)$$

## 2.2 Euler Angles and our Coordinate System

When describing rotating particles it is common to use the so called Euler Angles. A formal definition can be found at MathWorld [17] but for the purposes of this thesis we will describe it as a transformation from our stationary coordinate system  $\{x,y,z\}$  to the coordinate system attached to our particle  $\{x',y',z'\}$ . This transformation is done in three steps and using the intermediate axis T.

- Rotate the x-y plane  $\phi$  about the z-axis.
- Denote the shifted x axis T and rotate the z-y' plane  $\theta$  around this axis
- Rotate  $\psi$  around the z' axis to obtain the final coordinate system

This is illustrated in figure 2.2 where each prim marks one more step of rotation to the coordinate system. To make it clear how this relates to the experiment figure 2.3 shows the Euler angle rotations for a triaxial particle shown from a point of view similar to the of the experiment where the X-Z plane is the primary plane. This means we can describe the orientation of a particle using  $\mathbf{E} = (\phi, \theta, \psi)$ .

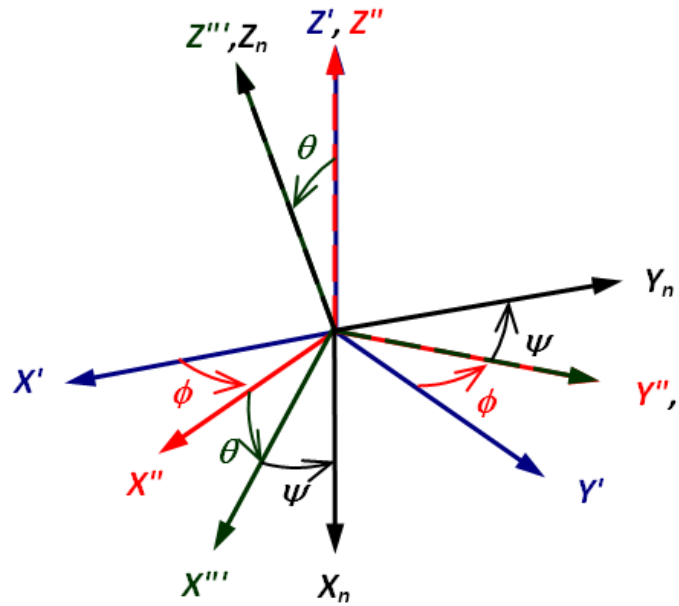


**Figure 2.2:** The Euler angles illustrated using a series of coordinate rotations. This is the normal way of illustrating the Euler angles as it is how they are defined.

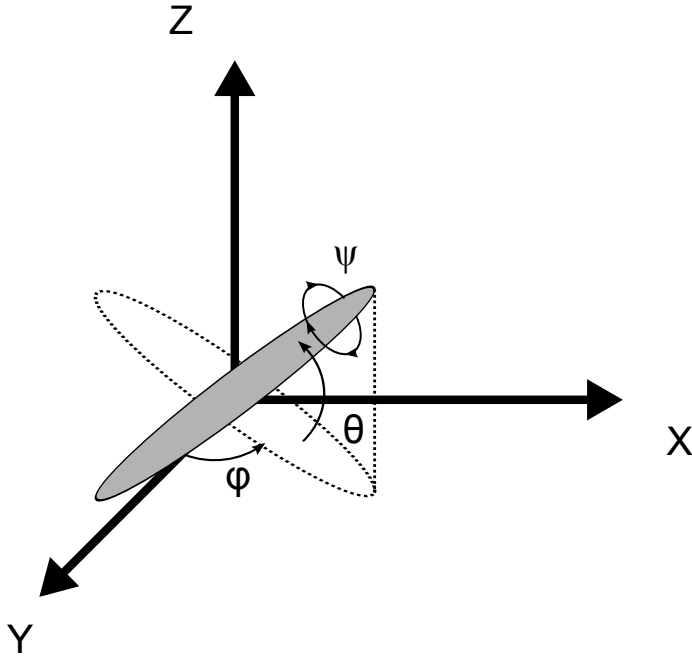


**Figure 2.3:** The Euler angles illustrated using an ellipsoid. This alternate visualization shows the angles with a point of view similar to that of the camera in the experiment. Note although  $\psi$  has an impact on the particle dynamics, as the particle is nearly axis-symmetric we can not observe it

### 2.2.1 Triaxial particles

Triaxial particles have, as the name suggests, three axis that are all distinct, compared to a sphere which has only one and an ellipse that has two. I will in this thesis refer to the lengths of these axes as  $a_x, a_y, a_z$  corresponding to their lengths along those axes for  $\mathbf{E} = (0,0,0)$ .

We are interested in the orientation of the particle

## 2.3 Jeffery Orbits

The Jeffery Orbit describe the motion of an ellipsoidal particle in Stokes shear flow as a function of time. The initial orbits found by Jeffery were for axis-symmetrical ellipsoidal particles, but was generalized by Yarin et al [7] to triaxial particles. Note that Jeffery Orbits sometimes refers only to the symmetric orbits but I will in this thesis refer to the generalized orbits as the Jeffrey Orbits. The generalized equations of motion found by Yarin et al was

$$\frac{d\theta}{dt} = (g_2 \sin \psi + g_3 \cos \psi) \sin \theta \quad (2.5a)$$

$$\frac{d\phi}{dt} = \frac{1}{2} + g_3 \sin \psi - g_2 \cos \psi \quad (2.5b)$$

$$\frac{d\psi}{dt} = g_1 + (g_2 \cos \psi - g_3 \sin \psi) \cos \theta \quad (2.5c)$$

(2.5d)

where the functions  $g_i$  are defined as

$$g_1 = \frac{a_y^2 - a_z^2}{2(a_y^2 + a_z^2)} \left( -\frac{1}{2}(\cos^2 \theta + 1) \sin 2\phi \sin 2\psi + \cos \theta \cos 2\phi \cos 2\psi \right), \quad (2.6a)$$

$$g_2 = \frac{a_z^2 - a_x^2}{2(a_x^2 + a_z^2)} (-\cos \theta \sin 2\phi \sin \psi + \cos 2\phi \cos \psi), \quad (2.6b)$$

$$g_3 = \frac{a_x^2 - a_y^2}{2(a_x^2 + a_y^2)} (\cos \theta \sin 2\phi \cos \psi + \cos 2\phi \sin \psi) \quad (2.6c)$$

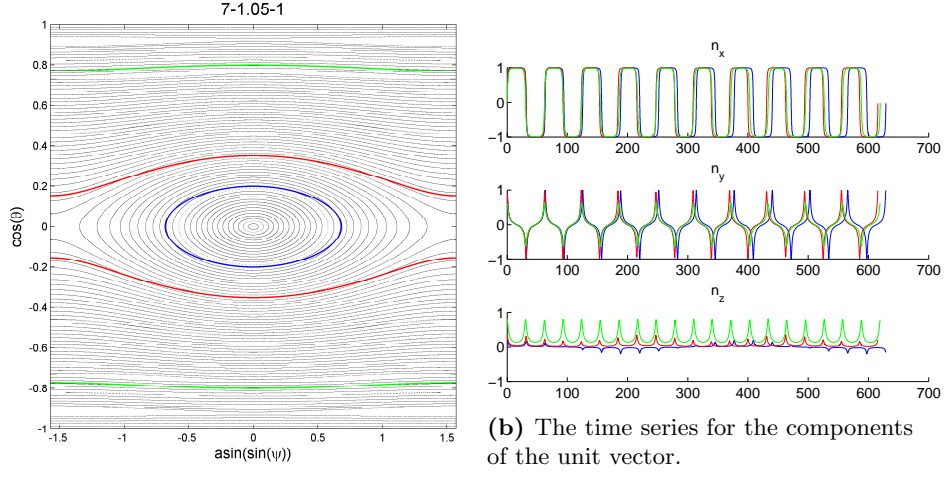
where the angles are defined as can be seen in figure 2.2. We can make a few key observations  
Solutions to the equations of motions can be found with numerical methods as shown by CITE  
SOME DUDE but one has to be careful to convert to the right coordinates.

The orbits for different initial conditions can be plotted in a Poincaré map, also known as a Surface of Section (S.O.S) [18] for  $\phi = 0$ . A few such maps can be seen in figure ???. A simplified explanation of the Poincare map is that a particle starting on some point on a line in the map will follow along that line the next time it intersects with the section, in our case when the particle has  $\phi = 0$ .

For a particle with a small asymmetry there are essentially three classes of orbits.

1. Periodic. For larger  $|\theta|$  there is little variation and the particle is largely periodic with fluctuations too small to measure.
2. Quasi-periodic bent: For intermediate  $|\theta|$  the amplitude of  $\cos(\theta)$  changes noticeably but does not change sign.
3. Quasi-periodic circular: For small  $|\theta|$  the amplitude of  $\cos(\theta)$  will change noticeably and change sign from positive to negative.

These three different types of orbits are illustrated in 2.4 and also shows .



(a) A poincare map

(b) The time series for the components of the unit vector.

**Figure 2.4:** A poincare map and three orbits for the Jeffery orbits of a particle with  $\lambda = 7$  and  $\epsilon = 0.05$ . The three orbits highlight the three different kinds of orbit, the quasi periodic circular orbit in blue, the quasi-periodic bent orbit in red and the periodic in green. We see that while  $n_x$  and  $n_y$

### 2.3.1 Winding Number

The quasi-periodic orbits are also referred to as double-periodic. This is referring to the fact that the variations that are seen in figure 2.4b are periodic as well. The ratio between the two periods is referred to as the winding number  $\omega$ , or simply

$$\omega = \frac{\theta_1}{\theta_2}. \quad (2.7)$$

which is illustrated in figure 2.5.

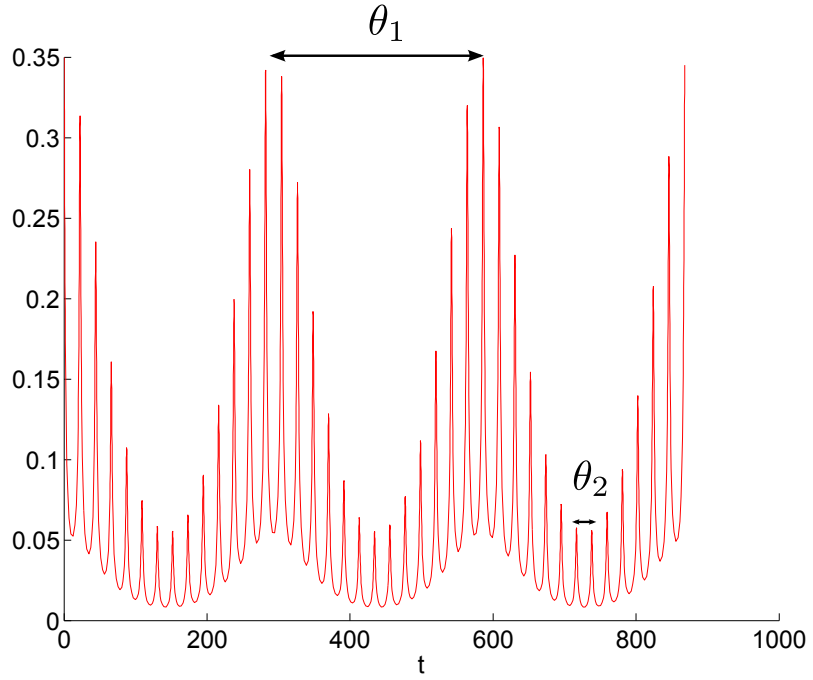


**Figure 2.5:** The winding number is defined as the quotient between the longer and shorter period. This is the  $n_z$  plot bent quasi periodic orbit from figure 2.4 highlighting the short period  $\theta_2$  which is simply the period of  $\phi$  and the longer period  $\theta_1$ .

This can also be thought of as the number of steps travelled on the poincare map before coming back to where it started, divided by the number of laps it takes. This number is the same for any point along a given orbit on the poincare map but varies greatly for different orbits as well as for different asymmetries. The winding numbers for orbits a slice along  $\psi = 0$  for  $\epsilon = \{0.01, 0.05, 0.10\}$  can be seen in figure 2.6

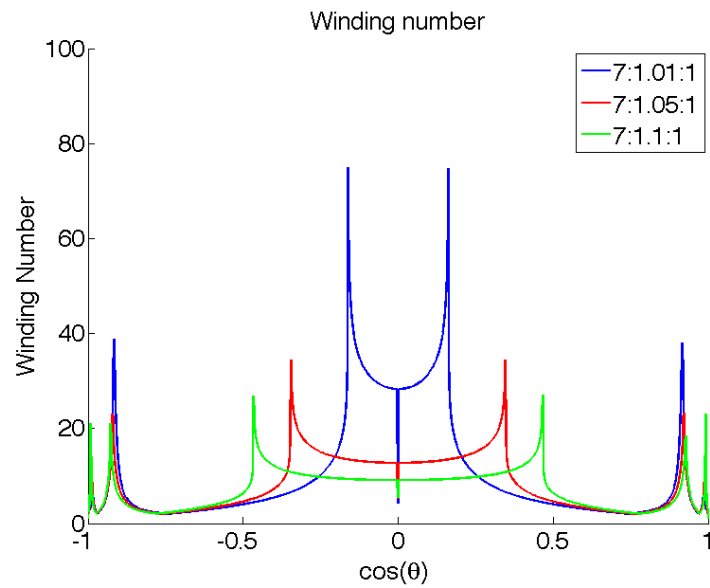


**Figure 2.6:** The winding number as a function of  $\cos(\theta)$  for three different asymmetries. The sharp edge that occurs centered around zero is when the circular orbits break into bent orbits as mentioned previously. We see that a lower asymmetry leads to a sharper difference between the circular and the bent orbits.

# 3

## Method

# **Part I**

## **Improvements of Experimental Setup**

### 3.1. IMPROVEMENTS

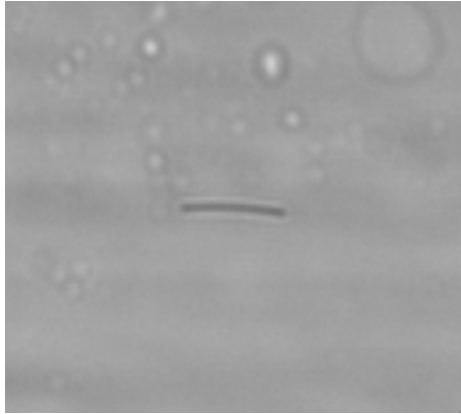
---

As previously mentioned this thesis is a continuation of work done by Mehlig, Einarsson and Mishra et al [1, 13, 19]. Their results were promising but there were a number of key limitations and problem that we want to solve to improve the results and the ease of getting results. Roughly they are

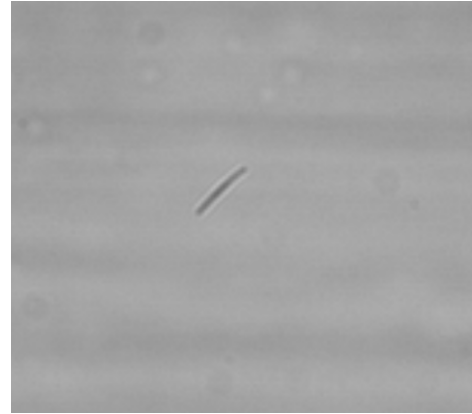
1. The particles
  - Very few particles are symmetric, most are visibly bent or uneven, see figure 3.1
  - Few particles have a low enough aspect to be useful.
  - Have greatly varying and difficult to measure width meaning the aspect ratio cannot be estimated well
  - Cannot be trapped with an optical tweezer due to low transmittance
2. The PDMS in the channel is very jagged which causes a great deal of noise unless the focus is in a very narrow band
3. Manual tracking of particles is time consuming and mentally draining.
4. Bubbles are difficult to avoid when setting up the experiment

## 3.1 Improvements

### 3.1.1 Particles and Channel



(a) Particle 13 from July 2012



(b) Particle 22 from July 2012

**Figure 3.1:** Two fairly typical particles from the previous setup. Note that these are still selected from the total pool of particles for being relatively symmetric and yet are noticeably bent.

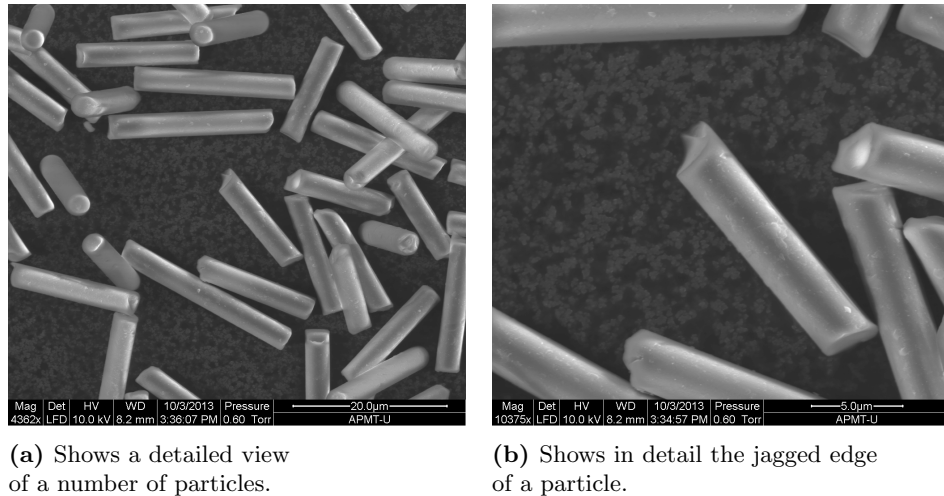
To solve the problems with the particles we replaced them with glass particles from Nippon Glass, Japan [20]. The particles are made from LCD spacing rods that are , which means they are essentially broken cylinders with very consistent width but quite varying length. Two different batches of particles have been used, one with  $3\mu m$  diameter and one batch with  $5\mu m$  diameter. All

### 3.1. IMPROVEMENTS

---

the particles presented in the results section are from the  $3\mu\text{m}$  batch. To verify that the particle were indeed as symmetric and with as even width as we suspected images were taken with an ESEM (Environmental Scanning Electron Microscope) and can be seen in figure 3.2. We see that the particles are uniformly smooth along the edges but have varyingly jagged edges causing different degrees of asymmetry.

In particular figure 3.3b shows a top down view of a particle clearly showing a very circular shape with no discernible asymmetry.



(a) Shows a detailed view  
of a number of particles.

(b) Shows in detail the jagged edge  
of a particle.

**Figure 3.2:** Pictures of the glass particles that particles

### 3.1. IMPROVEMENTS

---

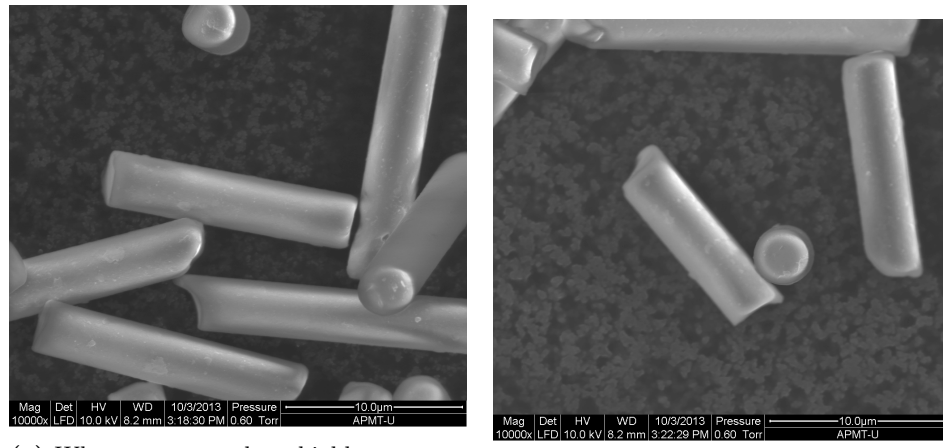


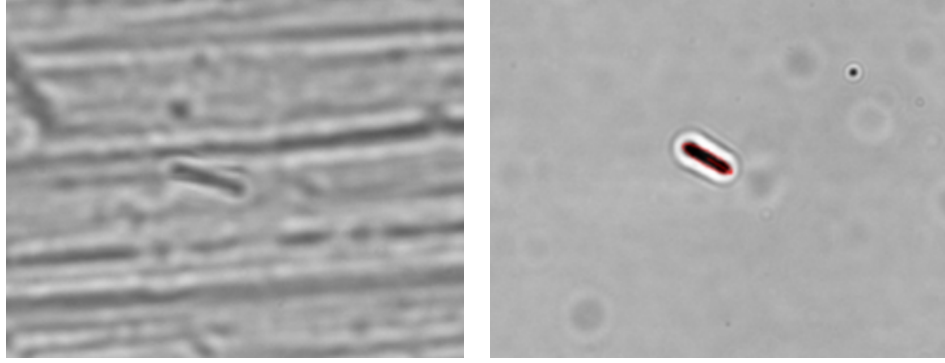
**Figure 3.3:** Pictures highlighting the roundness of the particles as well as the apparent symmetry of some particles. It should be noted that although there are no apparent rough edges there was no way to rotate a sample so there might very well be asymmetries on the side of the particle that we cannot see.

While these particles seemingly satisfy the symmetry conditions they are made glass with a density of approximately  $2.57 \text{ g/cm}^3$  at  $20^\circ\text{C}$  which is significantly higher than that of water with a density of  $1 \text{ g/cm}^3$  at  $20^\circ\text{C}$  and glycerol with a density of  $1.5 \text{ g/cm}^3$ . Thus to correct for the density and limit sinking or floating the water soluble Sodium metatungstate which at  $20^\circ\text{C}$  has maximum density of  $2.94 \text{ g/cm}^3$ . To increase the viscosity of the liquid around 8% glycerol is added, resulting in a measured dynamic viscosity of  $24 \cdot 10^{-3} \text{ Pa s}$

A problem in finding and tracking a particle was that the surface of the PDMS was very uneven and one could see sharp ridges along the length of the channel like in figure 3.4a unless the focus was in a relatively narrow depth of the channel.

### 3.1. IMPROVEMENTS

---



(a) An unusual severe case of the PDMS edges creating noise.

(b) After being polished there is no trace of such ridges.

**Figure 3.4:** Pictures highlighting the roundness of the particles as well as the apparent symmetry of some particles. It should be noted that although there are no apparent rough edges there was no way to rotate a sample so there might very well be asymmetries on the side of the particle that we cannot see.

This was fixed by polishing the copper mold in which the PDMS channels are formed with a silicate abbrasive (Autosol) and emery cloth. This reduces all visible scratches from the mold and thus from the PDMS and the result can be seen in figure 3.4b.

#### 3.1.2 Automated Tracking

One of the most time consuming aspects as well as mentally draining is manually tracking a particle. Depending on the flow rate and the number of stretches and runs desired for a particle it can take several hours. Thus one of the primary targets for improvement as discussed by Johansson [1] was to try and make the camera tracking automatic. This would enable faster measurements as well as more measurements since it would reduce fatigue.

Such a tracking was implemented using Python and the external packages `OPENCV`, `NumPy`, `SciPy`, `ImageMagick` and `ctypes`. The goal of the tracking is relatively similar to the tracking described in ?? and more in detail in Johansson [1] however there are a few very important differences that produce unique problems.

#### 3.1.3 Aquiring the image

The first step in this is to acquire the image from the microscope in order to identify (and track) the particle. However the Leica DFC350 FX camera only works with the proprietary Leica software which means there is no easy way to get this image straight from the camera in real time. This meant we were forced to use the `ImageGrabber` package in Python and then isolate the camera image from the screen. This quite easy to do but takes ca 50ms per frame which would be unnecessary for an open source camera software.

### 3.1.4 Removing noise

The first step is to reduce the static noise from the movie caused by dirt, scratches and other defects in the microscope and on the camera lens as can be seen in figure 3.7a. As the noise is static and everything else changes this is a simple matter of computing an average frame

$$\bar{F} = \frac{\sum_{n=1}^N F}{den} \quad (3.1)$$

an example of such an average frame can be seen in figure 3.7b. This is then removed from the camera frame and the result can be seen in figure 3.7c. After this we apply a smoothing function and Canny edge detection [?] and then fill the resulting edge.

### 3.1.5 Contour detection and selection

Once an edge image has been generated, the OCV package has another useful function, `Contours` which returns a list of every contiguous group of edge pixels. If we have chosen the threshold values to the edge detection correctly, this should include the particle or a good approximation of it.

In order to find the correct contour a few techniques are used.

First contours whose total size is less than some minimum value,  $n_{min}$  or larger than some maximum value  $n_{max}$  are ignored. Then the position  $P_i$  of each contour  $C_i = p_1, p_2, \dots, p_n$  is calculated as the average pixel position

$$P_i = \sum_j^n p_j / n$$

This position is compared to the expected position of the particle, which the very first frame is the middle position and thereafter is assumed to have constant speed.

Finally a 'thinness value' is calculated according to eq 3.2

$$w_{thin} \left( \frac{n}{d_{max}^2} \right)^2 \quad (3.2)$$

. where  $w_{thin}$  is a weighting constant,  $n$  is the number of pixels in the contour and  $d_{max}$  is the longest distance between two pixels in the

### 3.1.6 Adjusting the Camera velocity

Once detected twice the particle will have some velocity relative to the camera  $v_{rel}$  and a position  $\mathbb{P}$ . If the velocity is larger than some threshold  $v_{thresh}$  or the position is outside a center square in the image,  $\mathbb{P} \notin \mathbf{B}$  we want to adjust the velocity of the step engine.

We then simply do a straight correction but with a damping factor to prevent a feedback loop. So our resulting velocity change

$$V_c = v_{rel} \cdot \zeta \quad (3.3)$$

### 3.1.7 Time Considerations

A higher frame rate will allow for greater predictive power and increase stability as the error between frames is reduced. So reducing computational time of each task is important for optimizing the tracking which also means knowing what tasks are the most demanding. A list of the different tasks and their average execution times can be seen in table 3.1

Task	Average time	Std deviation
Capture screen	1000	200
Find edges	200	20
Change velocity	400	50

Table 3.1

We see that the FPS is limited primarily by three routines: The screen capture routine, the change velocity routine and finally the save position routine. The first and last are unavoidable and must be done every frame by definition if we are interested in knowing the particles position as well as possible. This means we simply want to use the velocity correction as little as possible. Since the time constraint is in the communication with the step engine, there is not any optimization to be done here, at least not within the scope of this thesis.

## 3.2 Experimental Setup

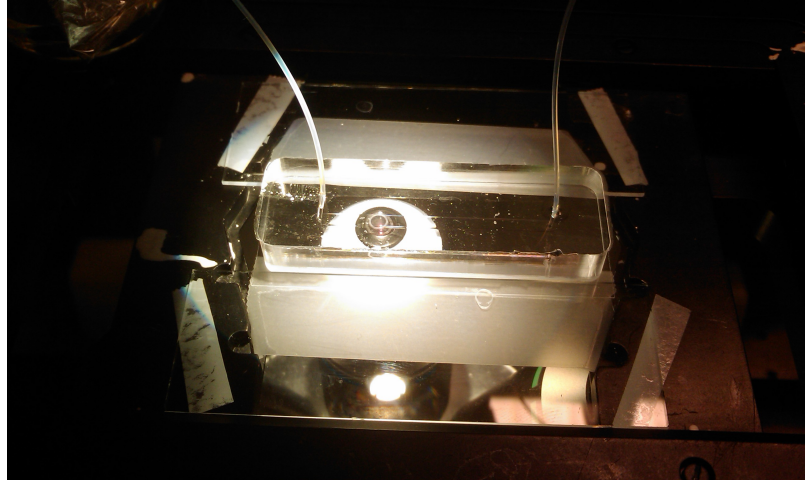
As the goal is to attempt to verify the Jeffrey equations in eq 2.5 we need an experimental setup with particles and flow system that satisfy the conditions that the Jeffrey equations apply under. This means our particles have to be buoyant, triaxially symmetric and small enough that inertial effects are negligible. The flow has to be a linear creeping flow, in other words have a Reynolds number satisfying  $Re \ll 1$  and have a high unidirectional shear that allows one to detect the orbits in a relatively short distance.

The particles used in previous measurements were made from epoxy mixed in a vortex[13] which made them buoyant and small enough to ignore inertial effects, but they were not symmetrical enough to produce reliable periodic Jeffrey orbits. Thus two sets of glass particles from Nippon Glass, Japan[20], have been used. They are cylindrical with a consistent width of  $3\text{ }\mu\text{m}$  and  $5\text{ }\mu\text{m}$  and varying length. Images taken with a STEM microscope can be seen in figure 3.2.

While these particles seemingly satisfy the symmetry conditions they are made of glass with a density of approximately  $2.57\text{ g/cm}^3$  at  $20\text{ }^\circ\text{C}$  which is significantly higher than that of water with a density of  $1\text{ g/cm}^3$  at  $20\text{ }^\circ\text{C}$  and glycerol with a density of  $1.5\text{ g/cm}^3$ . Thus to correct for the density and limit sinking or floating the water soluble Sodium metatungstate which at  $20\text{ }^\circ\text{C}$  has maximum density of  $2.94\text{ g/cm}^3$ . To increase the viscosity of the liquid around 8% glycerol is added, resulting in a measured dynamic viscosity of  $24 \cdot 10^{-3}\text{ Pa s}$

### 3.2. EXPERIMENTAL SETUP

---



This liquid with suspended particles is flowed through a channel of Polydimethylsiloxane (PDMS) 4 cm long, 2.5 mm wide and either 200  $\mu\text{m}$  and 500  $\mu\text{m}$ . The flow profile of such a channel was calculated by Anton Johansson in his thesis[1] and can be seen in figure 3.5. The flow rate varies between 2 and 20  $\mu\text{l}/\text{m}$  or in SI units  $3.33 \cdot 10^{-10} \text{ m}^3/\text{s}$  which with a cross section of at least  $5 \cdot 10^{-7} \text{ m}^2$  means a maximum flow speed of 6.66  $\text{mm}/\text{s}$ .

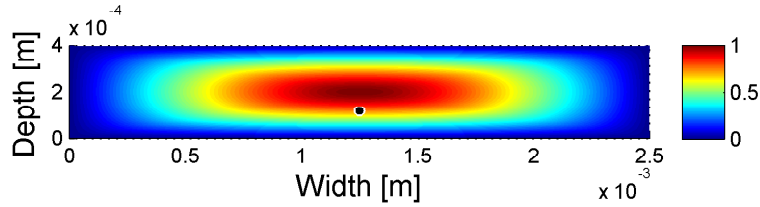


**Figure 3.5**

To confirm that the flow is a creeping flow we can calculate the maximum Reynolds number using eq 2.1 and our maximum flow speed

$$Re = \frac{UL\rho}{\mu} \leq \frac{6.66 \cdot 10^{-3} \cdot 2.5 \cdot 10^{-3} 2.5}{24 \cdot 10^{-3}} \approx 1.6 \cdot 10^{-3} \ll 1 \quad (3.4)$$

This should satisfy the conditions of the Jeffrey equations. To track the particles the channel is put in a moveable stage on a confocal microscope. The entire setup can be seen in figure 3.6

### 3.2. EXPERIMENTAL SETUP

---

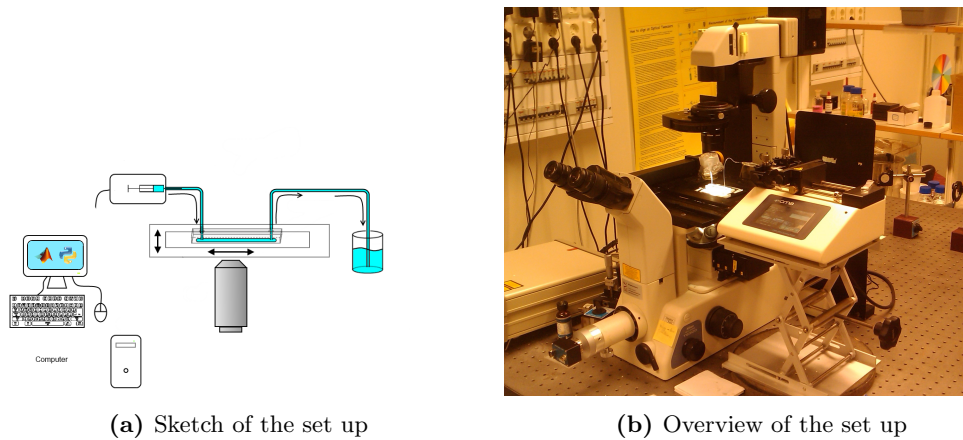


**Figure 3.6**

#### 3.2.1 List of equipment

- Leica DFC350 FX digital camera
- Nikon Eclipse TE 300 microscope
- Nikon 60x water immersion objective
- Märzhäuser Wetzlar 'LStep-eco' step engine
- CMA 4004 syringe pump

#### 3.2.2 Density matching

$$\rho_a = \frac{m_a}{V_a} = \frac{V_b \rho_b + V_{mix} \rho_{mix}}{V_b + V_{mix}} \quad (3.5)$$

So if we want to find  $V_{mix}$  we get

$$V_{mix} = \frac{V_b(\rho_b - \rho_a)}{\rho_a - \rho_{mix}} \quad (3.6)$$

## **Part II**

# **Measurements and Analysis**

### 3.3 Data Analysis

Once a movie had been recorded we want to estimate the dynamics of the particle. This is done in several steps.

#### 3.3.1 Particle identification

The first step is to reduce the static noise from the movie caused by dirt, scratches and other defects in the microscope and on the camera lens as can be seen in figure 3.7a. As the noise is static and everything else changes this is a simple matter of computing an average frame

$$\bar{F} = \frac{\sum_{n=1}^N F}{den} \quad (3.7)$$

an example of such an average frame can be seen in figure 3.7b. This is then removed from the camera frame and the result can be seen in figure 3.7c. After this we apply a smoothing function and Canny edge detection [? ] and then fill the resulting edge. The resulting pixels are then fit to an ellipse as described in [1? ]. The filled contour and the fit ellipse can be seen in figure 3.7d.

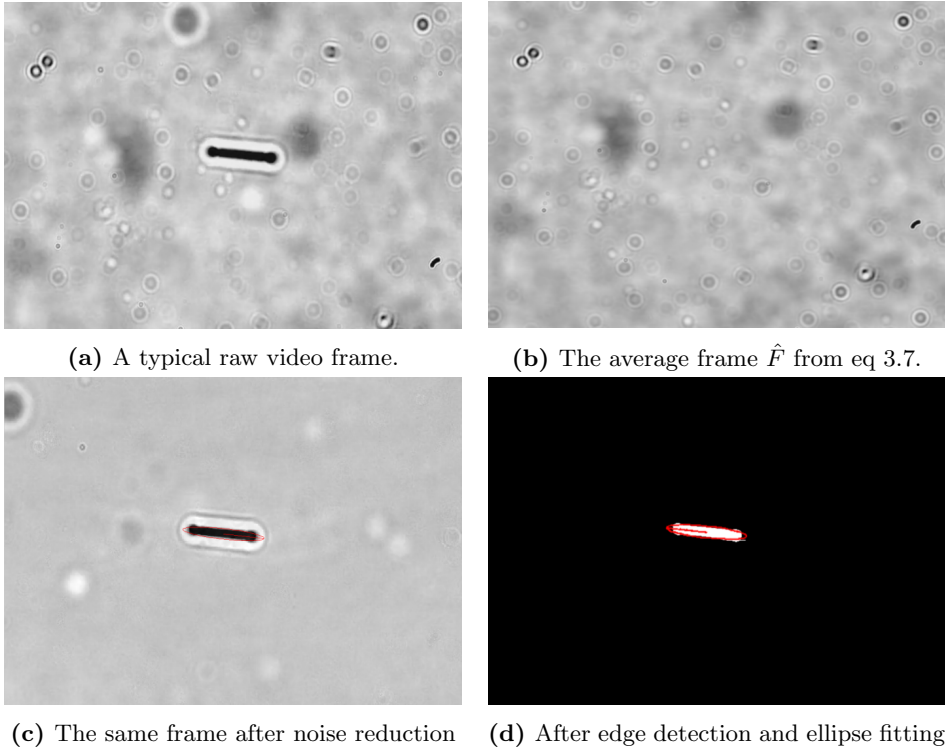


**Figure 3.7:** These pictures show a simplified version of the image analysis from raw image to estimated particle position

### 3.3.2 Estimation of orientation

The ellipsoid we get is then our best approximation of the projection of the actual particle. In order to normalize  $\mathbf{n}$  we need to know the length of the particle. However as it was shown by Leal that the particle will always spend a majority of its time aligned with the flow, ie aligned with the camera which means that by simply calculating the length  $L$  every frame and finding the mode of the distribution we will find a good estimate of  $L$ .

So given an ellipsoid with length  $l_e$ , width  $d_e$  and angle  $\phi_p$  we find

$$p_x = l_e * \sin(\phi_p) \quad (3.8)$$

$$p_z = l_e * \cos(\psi_p) \quad (3.9)$$

with x and z projection  $p_x$  and  $p_z$  we can get  $n_x$  and  $n_z$  as well as  $n_y$  via

$$n_x = \frac{p_x}{L} \quad (3.10a)$$

$$n_z = \frac{p_z}{L} \quad (3.10b)$$

$$n_y = \sqrt{1 - n_x^2 - n_z^2} \quad (3.10c)$$

### 3.3.3 Width compensation

Up until this point we have assumed that the particle is a *thin* rod so that the projection  $\mathbf{p}$  onto the x and z-axes give us an accurate estimate of  $\mathbf{n}$ . However when we are projecting 'thick' particle with length  $L$  and width  $D$  we get  $\mathbf{n}'$ . At  $\phi = 0$  this is

$$\mathbf{n}' = n'_z = n_z \cos(\theta) + D \sin(\theta) \quad (3.11)$$

which is illustrated in figure 3.8.

In order to compensate for this error we modify our projection equation 3.8 to

$$p_x = (l_e - w_e) * \sin(\phi_p) \quad (3.12)$$

$$p_z = (l_e - w_e) * \cos(\psi_p) \quad (3.13)$$

This will reduce the particles estimated length by  $w_e$

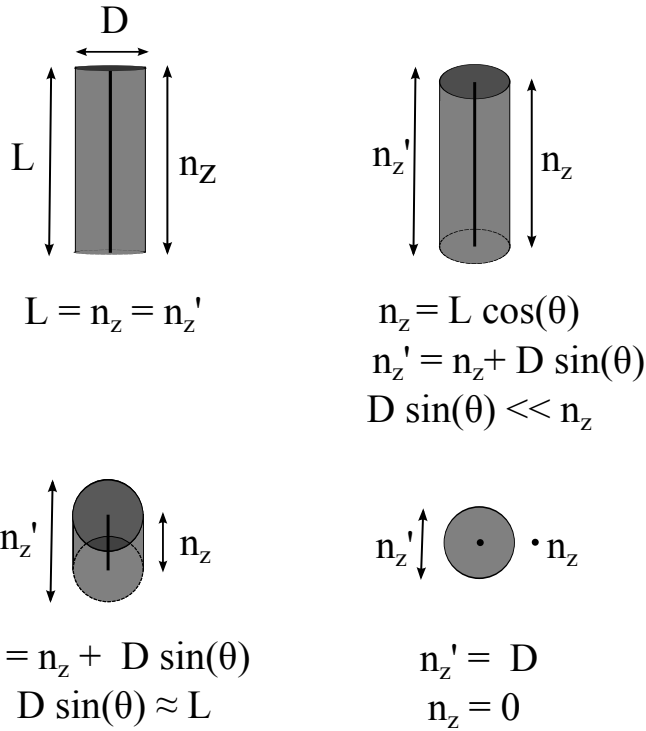


Figure 3.8

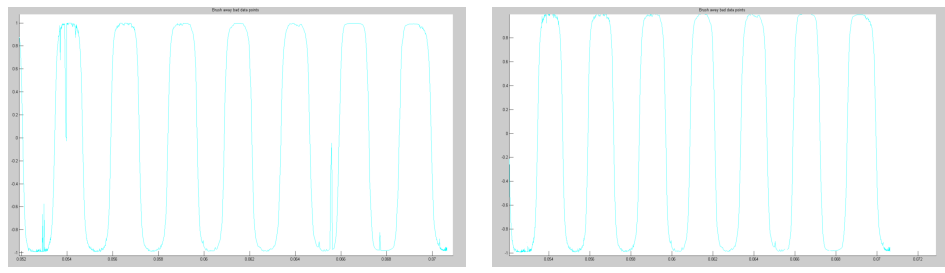
### 3.3.4 brushing

The tracking will typically have a few frames where either the particle is obstructed or is not detected correctly leading to spikes in the data. To make further theoretical analysis possible such points are removed manually. The basis for removal is simply a large discontinuity in the data, and while this could largely be eliminated with algorithmic means in particular for  $n_x$  it's very difficult to write an algorithm that will satisfactorily catch all possible edge cases. It's thus simpler to look at the analysis program and remove the points where the particle cannot be traced accurately due to noise.

An example of unbrushed and brushed data can be seen in figure 3.9 and all unbrushed data files will be available at [INSERTURLHERE](#)

### 3.3. DATA ANALYSIS

---



(a) Tracking data before brushing.

(b) tracking data after brushing.

**Figure 3.9:** Shows a set of data before and after removing points where a significant amount of noise disturbed the tracking.

#### 3.3.5 Winding number estimation

#### 3.3.6 Matching to theoretical orbit

# 4

## Results

During the work of this thesis around 300 movies of particles have been recorded with gradual improvements to the setup in terms of density matching, particle density, bubble elimination etc. In this section we will present the data from three movies of two different particles. One referred to as particle A, the other as particle B. The measurements in this section was done together with Alexander Laas.

### 4.1 Particle A

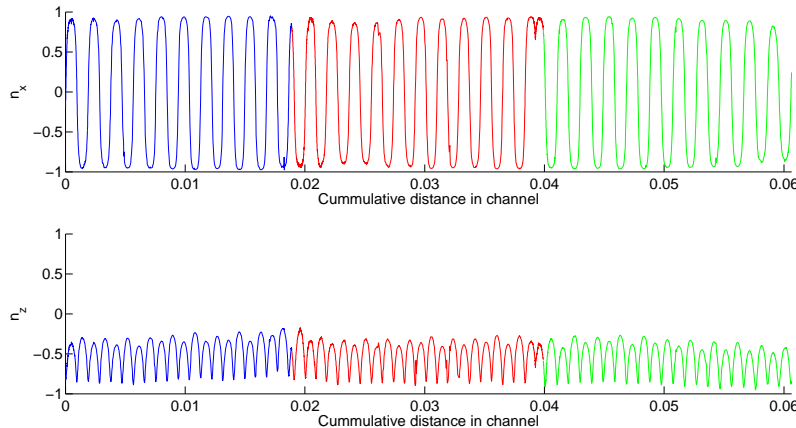


**Figure 4.1:** Low nz almost periodic.

#### 4.1. PARTICLE A

---

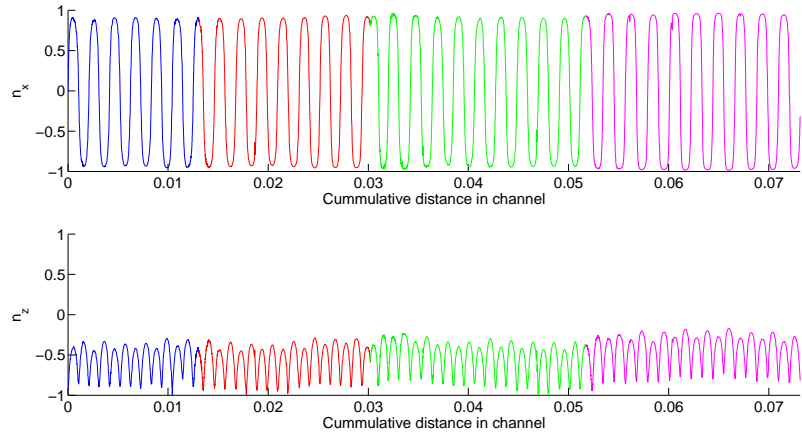


**Figure 4.2:** High nz very periodic.

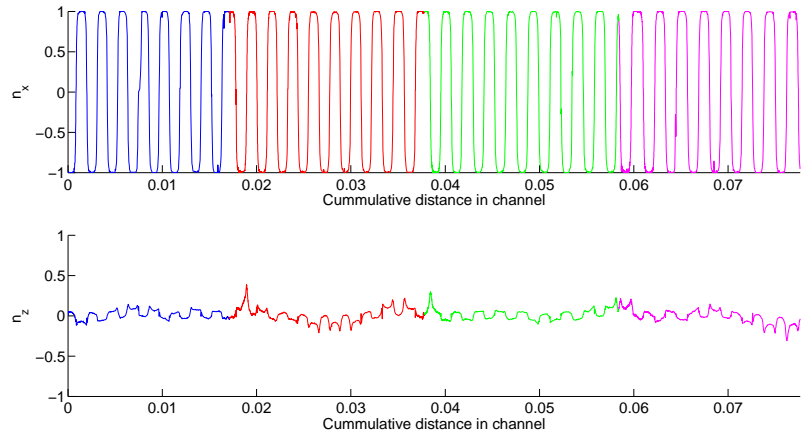


**Figure 4.3:** Low Nz odd reversals, first peaks is bad, rest are great.

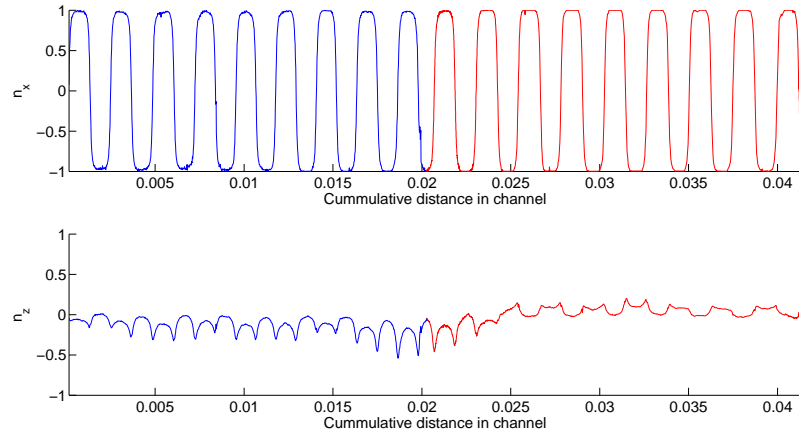


**Figure 4.4:** Low Nz bad reversal.

## 4.2 Particle B

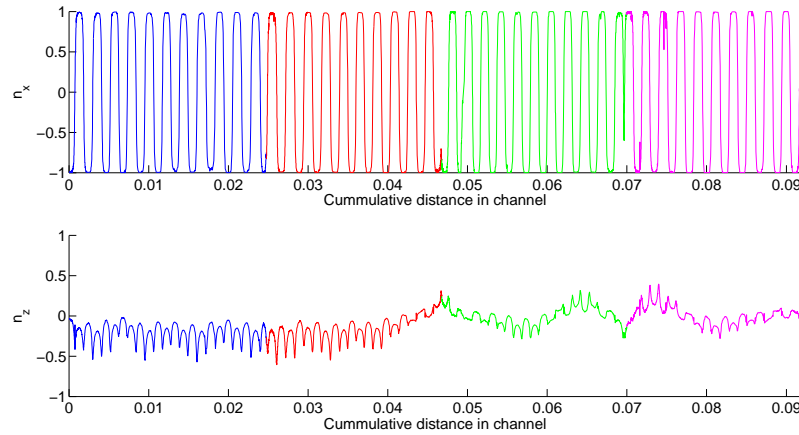


**Figure 4.5:** Low nz quasiperiodic.

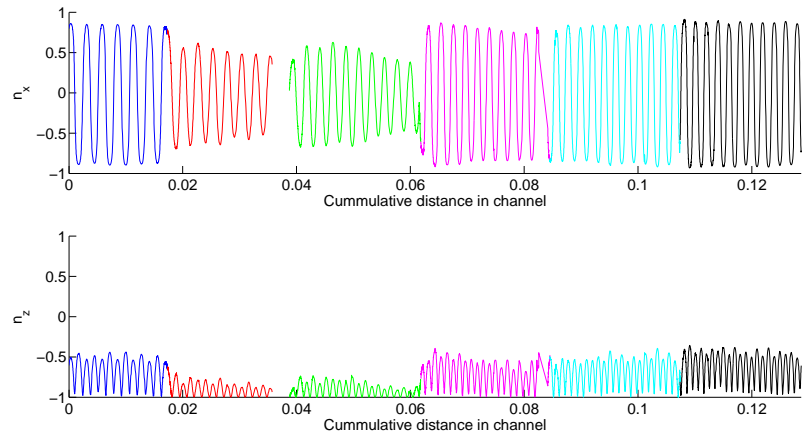


**Figure 4.6:** High nz periodic.

# 5

## Discussion

A

Raw data

# Bibliography

- [1] J. A., Analysis of empirical data on the tumbling of microrods in a shear flow, Master's thesis, Chalmers University of Technology.
- [2] E. J., Low reynolds number particle dynamics, Master's thesis, Chalmers University of Technology.
- [3] A. Einstein, A new determination of molecular dimensions, Annalen der Physik.
- [4] G. B. Jeffrey, The motion of ellipsoidal particles immersed in a viscous fluid, Proceedings of the Royal Society A 102.
- [5] P. J. Gierszewski, C. E. Chaffey, Rotation of an isolated triaxial ellipsoid suspended in slow viscous flow, Canadian Journal of Physics 56 (1) (1978) 6–11.
- [6] L. G. L. E. J. Hinch, Rotation of small non-axissymmetrical particles in a simple shear flow, J. Fluid Mech 92 (1979) 591–608.
- [7] I. V. R. A. L. Yarin, O. Gottlieb, Chaotic rotation of triaxial ellipsoids in simple shear flow, J. Fluid Mech vol 340 (1997) 83–100.
- [8] F. C. van den Bosch, lecture 1: Surfaces of section, Online material for course.
- [9] S. G. M. H. L. Goldsmith, The flow of suspensions through tubes i. single spheres, rods, and discs, Journal of colloid science (17).
- [10] D. K. O.G. Harlen, Orientational drift of a fibre suspended in a dilute polymer solution during oscillatory shear flow, J. Non-Newtonian Fluid Mech. 73 (1997) 81–93.
- [11] T. Kaya, H. Koser, Characterization of hydrodynamic surface interactions of escherichia coli cell bodies in shear flow, Phys. Rev. Lett. 103 (2009) 138103.
- [12] C. J. S. Petrie, The rheology of fiber suspensions, J. of non-newtonian fluid mechanics 87.
- [13] J. E. et al, Periodic and aperiodic tumbling of microrods advected in a microchannel flow, Acta Mechanica (2013) 1–9.

## BIBLIOGRAPHY

---

- [14] T. Pedley, Introduction to Fluid Dynamics, Department of Applied Mathematics and Theoretical Physics, University of Cambridge, Silver St., Cambridge CB3 9EW, U.K., 1997.
- [15] S. Childress, An Introduction to Theoretical Fluid Dynamics, Cambridge University Press, 2008, page 117 Starts the discussion of time reversibility of Stokes' Flow.  
URL [www.math.nyu.edu/faculty/childres/fluidsbook.pdf](http://www.math.nyu.edu/faculty/childres/fluidsbook.pdf)
- [16] G. K. Batchelor, An Introduction to Fluid Dynamics, Cambridge University Press, 1967, page 212 is definition of Reynolds Number, page 233 is Stokes Law.
- [17] W. E. W, Euler angles, from MathWorld—A Wolfram Web Resource. (2013).  
URL <http://mathworld.wolfram.com/EulerAngles.html>
- [18] J. Munkhammar, Poincare map (2013).  
URL [mathworld.wolfram.com/PoincareMap.html](http://mathworld.wolfram.com/PoincareMap.html)
- [19] J. E. e. a. Y. N. Mishra, A microfluidic device for studies of the orientational dynamics of microrods, Proc. SPIE 8251 2825109.
- [20] N. E. G. Co, Gap spacers for lcds: Microrods, [www.neg.co.jp/epd/elm/e\\_prd/other/others\\_01.pdf](http://www.neg.co.jp/epd/elm/e_prd/other/others_01.pdf).